Article

ANALYSIS OF CONJUGATED PROCESSES OF FILM EVAPORATION AND CONDENSATION IN A TUBULAR HEAT EXCHANGER†

Lazhar Merouani,[1] Said Abboudi,[2*] and Salim Boulahrouz[3]

1. Laboratory of Sensors Instrumentation and Processes, Abbas Laghrour University, Khenchela, Algeria
2. IRTES-M3M, Université de Technologie de Belfort-Montbéliard, Site de Sévenans, 90010 Belfort, France
3. Faculty of Sciences and Technology, Abbas Laghrour University, Khenchela, Algeria

***** Author to whom correspondence may be addressed.
E-mail address: said.abboudi@utbm.fr

†This article has been accepted for publication and undergone full peer review but has not been through the copyediting, typesetting, pagination and proofreading process, which may lead to differences between this version and the Version of Record. Please cite this article as doi: [10.1002/cjce.22677]

Received 26 March 2016; Revised 27 May 2016; Accepted 23 June 2016
The Canadian Journal of Chemical Engineering

DOI 10.1002/cjce.22677

ABSTRACT

This paper investigates coupled phase changes by forced convection from co-current flows of liquid films and vapour-air mixtures in a tubular heat exchanger. Evaporation occurs in the inner tube and condensation in the annulus region. Heat and mass transfers in the liquid films and the vapour-gas mixtures are described by the conservation equations of momentum, energy and diffusion. An appropriate change of coordinates is introduced in order to obtain a computational mesh with straight liquid-mixture interfaces along the walls. The governing equations are discretized by an implicit finite differences method and solved using an efficient numerical methodology. The distributions of axial velocity, temperature and vapour concentration in all regions of the tubes are determined from iterative procedures with a high convergence rate. The current analysis also provides the axial evolutions of film thicknesses, heat flux, condensation and evaporation rates in the whole domain. In addition, the effects of the inlet parameters of Reynolds number, relative humidity, pressure and liquid flow rate on the heat transfer characteristics, the evaporation and condensation rates are also investigated. This article is protected by copyright. All rights reserved

Keywords: condensation, evaporation, heat exchanger, liquid film, vapour-air mixture

INTRODUCTION

Heat and mass transfer processes through thin liquid films flowing along solid walls are of great theoretical and practical interest, because of their wide applications in many industrial systems such as heat exchangers, distillation systems and refrigeration. Many studies of film condensation or evaporation were conducted to analyse the evolutions of heat and mass transfer for various conditions.

In the case of natural convection, a previous study on laminar film evaporation and condensation in vertical ducts was performed by Yan and Lin.[1] A great enhancement in heat transfer due to the exchange of latent heat with phase changes was found. Some numerical investigations of liquid film evaporation were then carried out for fluid flows along inclined plates,[2] coaxial cylinders,[3] and vertical tubes.[4] The authors showed that the thermal transfer is dominated by the latent heat transfer at the liquid-air interface. Ben Jabrallah et al.[5] considered the evaporation of a water falling film in a closed cavity. They analysed the influence of the heat flux and the wall temperature on the liquid film. Cherif et al.[6] presented a study of film evaporation in a vertical channel. They showed that the evaporative cooling occurs especially for small heating flux and large air velocities. Ben Radhia et al.[7] studied the evaporation of a water film in a vertical annulus. They analysed the influence of the operating parameters on the evaporated water flux. Another model has been developed by Debbissi et al.[8] for a binary liquid film. They showed that, under some particular conditions, it is possible to evaporate more water than if the liquid film was made of pure water only.

Moreover, condensation processes were also extensively studied by many authors. Siow et al.[9,10] developed numerical and analytical models for laminar film condensation of vapour-air mixtures along flat plates. The effects of the inlet parameters on the condensation process were analysed. Belhadj et al.[11] considered a downward flow of an air-water system in a vertical channel. They showed that increasing the water film amount benefits the condensation rate. Dharma Rao et al.[12] performed a theoretical study of convective vapour condensation in a vertical tube. Results showed that the heat transfer coefficients and the condensation rate decrease considerably for high air concentration. Park and Kim[13] performed a numerical study of a vertical evaporating tube with two thin liquid films flowing along the wall. By limiting their calculation on the near entrance of the tube, they analysed the evaporation delay and the temperature inflection of the inner film. Li and Li[14] studied numerically the condensation of humid air flowing over a vertical plate. Their results indicated that it was not reasonable to neglect the condensate film thickness. Some other studies of condensation of vapour-air mixtures in a vertical tube by forced[15] and mixed convection[16] were also performed. The authors showed that the condensation rates are small due to high air mass

fractions. Dahikar et al.[17] performed experimental investigations of steam condensation in vertical pipes for a wide range of pressures and tube diameters. CFD simulations were carried out and compared with the experimental values. Ganguli et al.[18] presented a critical review of the most important investigations of steam condensation in a vertical tube. CFD simulations of the pressure drop and the heat transfer coefficient were performed and compared with experimental data. Merouani et al.[19] studied the condensation of steam–gas mixtures between two coaxial cylinders. They analysed the effects of the inlet conditions, the non-condensable gas and the tube size on the condensation process. Dehbi et al.[20] developed numerical models to simulate condensation in laminar and turbulent forced flows along a flat plate. Their simulations were then conducted for vapour -gas mixtures in closed vessels. Zhao et al.[21] developed a mathematical model of free convective condensation on a vertical plate. The obtained expressions of film thickness and heat transfer coefficient are similar to those of Nusselt's model. More recently, Dehbi[22] proposed a generalized best-estimate correlation for air-steam condensation in turbulent free convection for high pressures and steam fractions.

To our knowledge, all the studies available in the literature are restricted to situations where the evaporation or condensation processes occur separately. So, the aim of the present study is to investigate the combined processes of film evaporation and condensation in coaxial tubes. The governing equations are considered for all fluids including the complete boundary conditions and the axial variations of both films thicknesses along the tubes. The analysis of the effects of key factors on the heat and mass transfer characteristics also provides useful results for the design of evaporators-condensers, heat exchangers and other systems used in some particular fields such as desalination, nuclear power plants and petroleum refining. Moreover, although the analysis is performed for coaxial tubes, the obtained results may be extended to other types of exchangers.

PHYSICAL MODEL

The physical model under consideration is a heat exchanger composed of two coaxial vertical cylinders with radii R and R' (Figure 1). Laminar co-current flows of vapour-air mixtures enter the inner tube and the annulus with uniform values of velocity, temperature, pressure and vapour mass fraction. The external wall is dry and insulated while the inside and outside walls of the inner tube are wetted by thin liquid films. In our operating conditions, condensation occurs at the outside region since the inlet vapour concentration is higher than the corresponding saturation value at the wall temperature. However, at the inside wall, the opposite conditions prevail and evaporation takes place in this region with a falling liquid film of decreasing thickness. A cylindrical coordinates system (Orz) is chosen with the following assumptions:

- Fluid flows are laminar, steady and two-dimensional;

- The boundary layer approximations are valid for liquid films and vapour-air mixtures;
- The pressures are uniform in the radial direction;
- The vapour-gas mixtures are assimilated to ideal gases;
- The temperatures of the liquid-mixture interfaces are equal to the local vapour saturation temperature.

GOVERNING EQUATIONS

With the above assumptions, the conservation equations of mass, momentum, energy, and diffusion are given below:

- Continuity equations:

$$\frac{\partial(\rho_k U_k)}{\partial z} + \frac{1}{r}\frac{\partial(r\rho_k V_k)}{\partial r} = 0 \qquad (1)$$

- Conservation equations:

$$\rho_k\left(U_k\frac{\partial \psi_k}{\partial z} + V_k\frac{\partial \psi_k}{\partial r}\right) = \frac{1}{r}\frac{\partial}{\partial r}\left(r\Gamma_{\psi k}\frac{\partial \psi_k}{\partial r}\right) + S_{\psi k} \qquad (2)$$

Where k = L for liquid films, k = M for vapour-gas mixtures. Expressions of variables ψ_k (U_k, T_k, C), diffusion coefficients $\Gamma_{\psi k}$, and terms $S_{\psi k}$ are given in Table 1.

In addition, the mass flow rate equations in the inner tube and the annulus are also written as follows:

$$\int_0^{R_i} \rho_M U_M 2\pi r.dr + \int_{R_i}^{R} \rho_L U_L 2\pi r.dr = q_0 + q_{L0}, \quad q_e = \int_0^z J_v 2\pi R_i dz \qquad (3a\text{-}b)$$

$$\int_{R+e}^{R'_i} \rho'_L U'_L 2\pi r.dr + \int_{R'_i}^{R'} \rho'_M U'_M .2\pi r.dr = q'_0, \quad q_C = \int_0^z J'_v 2\pi R'_i dz \qquad (4a\text{-}b)$$

q_0, q'_0 and q_{L0} are the inlet flow rates of the vapour-gas mixtures and the inner liquid, q_e and q_C are the accumulated flow rates by evaporation and condensation, J_v and J'_v are the vapour mass flux at the liquid-mixture interfaces.

BOUNDARY CONDITIONS

- At the inlet (z = 0), velocity, pressure, temperature and vapour mass fraction profiles are assumed to be flat for the inner and outer mixtures:

$$U_M = U_0,\ P_M = P_0,\ T_M = T_0,\ C = C_0 \qquad (5a–d)$$

$$U'_M = U'_0,\ P'_M = P'_0,\ T'_M = T'_0,\ C' = C'_0 \qquad (6a–d)$$

For the inner liquid film:

$$\delta(0) = \delta_0,\ T_L = T_{L0} \qquad (7a–b)$$

The inlet liquid velocity is calculated by neglecting convective and pressure terms in the momentum equation:

$$U_{L0} = \frac{g\rho_L}{4\mu_L}\left[R^2 - r^2 + 2(R-\delta_0)^2 \ln(r/R)\right] \qquad (8)$$

- On the axis, the symmetry conditions allow us to write:

$$\frac{\partial U_M}{\partial r})_0 = 0,\ \frac{\partial T_M}{\partial r})_0 = 0,\ \frac{\partial C}{\partial r})_0 = 0 \qquad (9a–c)$$

- At the liquid-mixture interfaces, continuity of velocity, shear stress, temperature, heat flux, diffusion mass flux and Fick's law are respectively imposed using:

$$U_L = U_M,\quad \mu_L \frac{\partial U_L}{\partial r})_i = \mu_M \frac{\partial U_M}{\partial r})_i \qquad (10a–b)$$

$$T_L = T_M,\quad -\lambda_L \frac{\partial T_L}{\partial r})_i = -\lambda_M \frac{\partial T_M}{\partial r})_i + J_v L_e \qquad (11c–d)$$

$$J_v = \rho_L\left(V_L - U_L \frac{d\delta}{dz}\right)_i = \rho_M\left(V_M - U_M \frac{d\delta}{dz}\right)_i,\quad J_v = -\frac{\rho_M D_v}{1-C_i}\frac{\partial C}{\partial r})_i \qquad (12e–f)$$

The saturated vapour concentration is calculated by the Gibbs-Dalton relation for ideal gas mixture:

$$C_i = \frac{M_v P_{vs}}{M_v P_{vs} + M_a (P - P_{vs})} \qquad (13)$$

- At the inner wall (internal and external side), the conditions of liquid adherence and continuity of temperature and heat flux give:

$$U_L = 0,\ U'_L = 0,\ T_L = T_S,\ T'_L = T_{S'}, \qquad (14a–d)$$

$$\lambda_L \frac{\partial T_L}{\partial r})_S = \lambda_S \frac{\partial T_S}{\partial r})_S,\quad \lambda_S \frac{\partial T_S}{\partial r})_{S'} = \lambda'_L \frac{\partial T'_L}{\partial r})_{S'} \qquad (15a–b)$$

- At the outer wall, the conditions of no-slip, insulated and impermeable wall are imposed:

$$U'_M = 0,\ \frac{\partial T'_M}{\partial r})_{R'} = 0,\ \frac{\partial C'}{\partial r})_{R'} = 0 \qquad (16a–c)$$

SOLUTION PROCEDURE

In order to accurately locate the liquid-mixture interface, the following transformation of coordinates is applied:

$$\eta_M = \frac{r}{R-\delta} - 3, \quad \eta_L = \frac{r-R}{\delta} - 1, \quad \eta_S = \frac{r-R}{e} - 1,$$

$$\eta'_L = \frac{r-R-e}{\delta'}, \quad \eta'_M = 1 + \frac{r-R-e-\delta'}{R'-R-e-\delta'}, \quad z' = z \qquad (17a–f)$$

In this new coordinates system, the positions of the inner and outer liquid-mixture interfaces correspond respectively to the values $\eta = -2, 1$ in the whole domain. The governing equations are then rewritten with these new coordinates and discretized on a structured grid by using an implicit finite difference method. The generated mesh is built with five different radial space steps $\Delta\eta_M$, $\Delta\eta_L$, $\Delta\eta_S$, $\Delta\eta'_L$, $\Delta\eta'_M$ in each phase (respectively internal mixture, internal liquid film, solid wall, external liquid film, external mixture). In order to obtain a greater node density near the leading edge, a small axial step size Δz_1 is used at the inlet due to higher gradients in this region. After a short distance, a higher step size Δz_2 is used on the remaining length of the tube (Figure 2). In the axial direction, the space derivative terms are approximated by a backward difference scheme (first order of truncation error). In the radial direction, central, backward and forward difference approximations are used respectively for internal and border nodes (second order of discretization). After rearrangement of terms, the resulting equations including four mesh nodes (represented by the subscripts W, E, P, N) may be written in the following general expression:

$$a_W \psi_k(W) + a_P \psi_k(P) + a_E \psi_k(E) + a_N \psi_k(N) = S_{\psi k} \qquad (18)$$

where a_w, a_E, a_P, and a_N are the coefficients of the variables $\psi_k = (U_k, T_k, C)$ at the nodes W, E, P, N (Figure 2), and $S_{\psi k}$ are the source terms in the governing equations.

As the transfer differential equations in both phases are parabolic, a marching scheme along the axial direction is used. So, the problem is solved line by line by applying an iterative method using the tri-diagonal matrix algorithm for energy and diffusion equations. The momentum equations in the liquid films and the mixtures associated with the equations of mass flow rate conservation are solved using the Gauss algorithm to obtain the axial velocity distributions and the pressure gradient. The radial velocity is calculated from the continuity equations. The evolutions of the liquid films thicknesses are also determined by an iterative procedure using the secant method for the relative errors on the liquid mass flow rates in both films. Moreover, an under relaxation technique is used in order to avoid oscillation or divergence of the solution during the iterative procedure, with an under relaxation coefficient equal to 0.2 for radial velocity and 0.4 for all other variables. The

numerical solution is considered well converged when the relative difference of the values of all variables ψ_k at all nodes between two successive iterations is less than 10^{-5}.

VALIDATION OF NUMERICAL MODEL

As it is previously mentioned, there are no similar studies of combined processes of film evaporation and condensation in the literature. So, it was not possible to perform a complete validation of our results in comparison of available studies. Thus, we considered two separate cases of film evaporation and condensation from steam-air mixtures. A first study is performed with a problem of film evaporation in a vertical tube with insulated wall. By comparing the calculated evaporation rates obtained by Feddaoui et al.[4] and the present model, we note that the agreement is overall satisfactory since the relative error is less than 2.5 % (Figure 3).

A second validation test is confirmed by comparison with the results of Dharma Rao et al.[12] for condensation of a saturated steam-air mixture. The evolutions of the Nusselt number and the heat transfer coefficient are compared with the present model. From Figure 4, it can be seen that these results are in good agreement, since the maximum errors are respectively 5.8 % for the heat transfer coefficient and 3.6 % for the Nusselt number. Thus, the numerical model can be effectively considered to be suitable for the present problem.

Furthermore, mesh independence tests were also performed with several grids in the following ranges: $28 \leq (N_M, N'_M) \leq 50$, $10 \leq (N_L, N'_L, N_S) \leq 20$, $100 \leq M' \leq 400$, $450 \leq M'' \leq 1800$, where N_M, N'_M, N_L, N'_L, N_S are the numbers of nodes in the radial direction and M', M'' in the axial direction. By comparing the values of the Nusselt number obtained from these grids, it was found that the relative errors are less than 1.5 % for all grids. We also noted that the relative difference obtained with the following grid: $(N_M, N_L, N_S, N'_L, N'_M) = (40, 16, 10, 16, 40)$, $(M', M'') = (200, 900)$ is less than 0.5 % compared to the finest mesh. Thus, it was deemed to be sufficiently accurate for our simulation conditions and used for all calculations performed in this study.

RESULTS AND DISCUSSION

In this study, the following fluids were considered: liquid water and steam-air mixtures. Their thermophysical properties are calculated from empirical and theoretical equations or by interpolation of tabulated data in the literature.[23] Calculations were first performed for the following conditions:

Dimensions: $R = 0.02$ m, $R' = 0.035$ m, $L = 1$ m

Inner tube: $P_0 = 100$ kPa, $Re_0 = 1500$, $T_0 = 85$ °C, $\varphi_0 = 0.5$, $C_0 = 0.2$, $\delta_0 = 0.095$ mm, $T_{L0} = 85$ °C, $q_{L0} = 1$ g/s

Annulus: $P'_0 = 100$ kPa, $Re'_0 = 1500$, $T'_0 = 95$ °C, $\varphi'_0 = 0.95$, $C'_0 = 0.714$, $\delta'_0 = 0$

Solid wall: e = 0.5 mm, $\lambda^* = 10$

Local Field Distributions

Figures 5-6 show the velocity profiles plotted at different sections z^* varying from 1 to 50 in the inner tube and the annulus. At the inlet, a thin liquid film is fed with an inlet flow rate q_{L0} in co-current downstream laminar flows of steam-air mixtures with uniform velocity profiles. In all our operating conditions, the outer fluid has higher values of temperature and vapour concentration than the inner mixture. So, under the simultaneous effects of vapour mass fraction and temperature gradients, evaporation occurs at the free surface of the inner film. The other side of the tube is below the vapour saturation temperature leading to vapour condensation on the wall. A thin liquid film flows downward on the outside surface of the tube with increasing values of flow rate and thickness while the mixture velocity decreases suddenly at the walls. Hence, along the liquid-mixture interface and the insulated wall, kinematic boundary layers are formed with high velocity gradients near the leading edge. In this region, the mixture velocity is much higher than that of the condensing film and decreases gradually while the liquid velocity increases under the combined effects of condensation and gravity. From an approximate distance $z^* = 20$, the mixture profile becomes nearly parabolic with a maximum velocity nearly located at $\eta = 1.45$.

In the inner tube, the opposite processes occur. Indeed, during the fluid flows, the film thickness and the velocity profiles of the evaporating liquid film decrease highly while the mixture velocity profiles increase significantly along the tube. They tend to parabolic distributions approximately from the section $z^* = 50$. Moreover, all fluid flows remain laminar, since their final Reynolds numbers are sufficiently low at the exit of the tubes ($Re_M = 2430$, $Re_L = 41$, $Re'_L = 12.7$, $Re'_M = 1215$).

Figures 7–8 show the temperature profiles in the whole domain and vapour concentration of the mixtures, plotted at the same sections. At the inlet, they are assumed uniform but are subjected to sudden changes at the walls. The onset of thermal and mass gradients leads to condensation and evaporation processes along the free surfaces of liquid films. Thus, the temperature and vapour concentration profiles increase gradually in the inner tube and decrease in the annulus along the flows while remaining maximum at the insulated outer wall and minimum at the inner tube axis. Moreover, it can be noted that the mixture profiles of both variables are almost similar along the tube. Their axial variations lead to a net reduction of the evaporation and condensation rates with a simultaneous heating of the internal fluid and cooling of the external fluid. In the liquid films and the solid wall, the temperature variations are smaller and the temperature profiles are almost linear. Finally, all profiles tend progressively to uniform values corresponding to isothermal saturation at the final equilibrium temperature which is not yet reached at the tube end (Figures 7–8).

Effect of the Inner Reynolds Number Re_0

The effects of various operating conditions on the hydrodynamic and thermal parameters are presented below. In order to analyse the influence of the inlet Reynolds number on the process, calculations are performed for Re_0 varying between 800 and 1800 corresponding to laminar flows of a saturated steam-air mixture.

Results presented in Figures 9–11 show the axial evolutions of the inner and outer film thicknesses, the evaporation and condensation rates, and the heat flux through the wall. An increase of Re_0 leads to an increase of inlet velocity and mixture flow rate with higher amount of air. Indeed, the slopes of curves increase highly with Re_0 near the inlet region. Consequently, the inner film thickness decreases significantly while the evaporation rate, the heat flux and the outer film thickness obtained by condensation increase with Re_0 at any axial location of the tube. Indeed, it can be seen from Figure 9 that for Re_0 varying from 800 to 1800, the inner film thickness is reduced by 9.4 to 11.4 % and its flow rate by 21.4 to 27 % at the exit of the tube.

Moreover, as the thermal flux is mainly due to the latent heat of phase change, it is almost proportional to the condensate mass flow rate. In steady state, the heat flux produced in the annulus from the outer condensing film is transmitted to the inner liquid film subject to heating and evaporation. Thus, for higher Reynolds number, more vapour flow rate is condensed in the annulus, more heat flux is produced by the outer film, and more water flow rate is evaporated in the tube and discharged by the inner mixture.

Effect of the Inner Relative Humidity φ_0

The effect of the inlet relative humidity is also examined for the inner steam-air mixture by varying φ_0 from 0 (dry air) to 0.9 (highly saturated air), corresponding to a range of inlet vapour concentrations C_0 between 0 and 0.4. Results presented in Figures 12-14 show the important effect of φ_0 on the transfer processes. As the inlet temperature is maintained constant (T_0 = 85 °C), an increase in φ_0 affects the inlet thermophysical properties of the mixture, leading to an increase in the partial vapour pressure, the steam mass flow rate and the inlet vapour mass fraction C_0 for constant values of all other parameters. Consequently, the steam mass fraction gradients at the interface decrease significantly with φ_0 leading to a net reduction of the evaporation rate and a slower decrease of the inner film thickness. This evolution of the evaporation process requires less heat flux which is coming from the external fluids and tends to restrict the condensation process in the annulus. It follows a more moderate increase of the outer film thickness, the condensate flow rate and the resulting thermal flux at the wall.

Effect of the Inner Pressure P_0

The effect of the inlet pressure of the inner mixture was investigated by varying P_0 from 75 to 150 kPa. In order to keep constant the inlet values of temperature and vapour concentration (T_0 = 85 °C, C_0 = 0.2), it was necessary to vary the inlet relative humidity between 0.374 and 0.746 while all other parameters remain unchanged. Therefore, an increase of P_0 leads to higher values of the mixture density, the partial pressure of air and vapour. In addition, as Re_0 is also maintained constant, it follows a decrease of the inlet mixture velocity. Consequently, the inner evaporation rate decreases significantly, leading to a slower reduction of thickness and flow rate of the inner liquid film (Figures 15–17).

On the other side, the condensate mass flow rate and the thermal flux due to vapour condensation increase when P_0 decreases, as shown in Figures 16–17. For low pressures, they reach high values which have the effect to promote the heat and mass transfer at the liquid-mixture interfaces. Indeed, in the inner tube, for small values of the pressure, the inner film may become completely dried out before the tube exit. However, in our operating conditions, this case has not been encountered in this study.

Effect of the Inlet Liquid Flow Rate q_{L0}

The effect of the inlet liquid flow rate was also investigated in the range between 0.5 and 2 g/s corresponding to an inlet film thickness δ_0 varying from 0.076 to 0.12 mm. Figure 18 shows that the accumulated evaporation rate increases significantly for low values of the feed water flow rate. Indeed, for q_{L0} = 0.5 g/s, the value of M_e exceeds 0.5 at the exit of the tube. From Figures 19–20, we can notice that the evaporated flow rate varies very slightly with the feed flow rate while the condensation rate and the total heat flux increase with q_{L0}. Indeed, the thermal flux due to heat transfer is produced by the simultaneous processes of vapour condensation and cooling of the external fluid in the annulus. It is then used for both heating and evaporation of the inner film, i.e. sensible and latent heats. So, an increase of q_{L0} requires a greater heat flux from the annulus to the inner film. As the evaporated flow rate and the latent heat flux are little affected by the variation of q_{L0}, it follows that the increase in the heat flux is completely caused by the sensible heat which is used for heating of a greater flow rate of feed water.

Finally, we note that for some particular conditions (low feed flow rate and high length of tubes), the inner liquid film thickness can be zero near the tube exit. In this case, the evaporating liquid phase disappears and our numerical model is no longer valid in this region. So, for future work, an extension of this study may be considered for a more complete analysis of this phenomenon.

CONCLUSION

A numerical investigation is conducted to study the coupled evaporation and condensation processes of thin liquid films flowing downward with steam-air mixtures in two coaxial tubes. The mathematical model developed is based on the conservation equations of mass, momentum and energy in all fluids and vapour diffusion in the mixtures. The evolutions of the liquid film thicknesses are calculated by iterative procedures using the mass balance equations at the liquid-mixture interfaces. The governing equations are discretized using an implicit finite difference method. Grid independence and validation tests of the numerical model were also performed.

Detailed results are presented including radial profiles of velocity, temperature, vapour concentration and axial evolutions of film thicknesses, heat flux, evaporation, and condensation rates. The main conclusions of this study can be summarized as follows:

- The onset of simultaneous processes of inner evaporation and outer condensation is caused by the coupled effects of thermal and mass gradients at the fluid interfaces.
- The evaporation and condensation processes in the tubes are highly coupled since the latent heat of condensation of the outer film is used to evaporate the inner film after passing through the solid wall.
- The condensate film thickness, the evaporation rate and the heat flux increase sharply at the inlet of the tubes, and tend gradually to a limit state corresponding to the thermal equilibrium in both tubes.
- These parameters also increase with the Reynolds number and decrease with the relative humidity and the pressure of flowing fluids in the inner tube.
- By increasing the inlet liquid flow rate, the evaporation rate is significantly reduced. However, the condensation rate and the heat flux are slightly improved with the inlet liquid flow rate.
- For some particular conditions (high length of tubes), the inner liquid film may disappear leading to a dry inner wall. In addition, the inner flow may become turbulent from some distance along the tube. So, further investigations are needed for future studies.

NOMENCLATURE

a_k	thermal diffusivity ($m^2.s^{-1}$)
C	vapour concentration ($kg.kg^{-1}$)
c_p	specific heat ($J.kg^{-1}.K^{-1}$)
D_v	diffusion coefficient ($m^2.s^{-1}$)
e	thickness of inner wall (m)
g	gravity acceleration ($m.s^{-2}$)
h	heat transfer coefficient ($W.m^{-2}.K^{-1}$)
J_v	local mass flux ($kg.m^{-2}.s^{-1}$)

L	height of tube (m)
L_c	latent heat of condensation ($J.kg^{-1}$)
L_e	latent heat of evaporation ($J.kg^{-1}$)
M_k	molar mass ($kg.mol^{-1}$)
M_c	condensation rate $M_c = q_c/q_{v0}$
M_e	evaporation rate $M_e = q_e/q_{L0}$
Nu	local Nusselt number
P	pressure (Pa)
q	mass flow rate ($kg.s^{-1}$)
r	radial coordinate (m)
R, R'	radii of cylinders (m)
Re	Reynolds number
T	temperature (K)
U	axial velocity ($m.s^{-1}$)
V	radial velocity ($m.s^{-1}$)
z	axial coordinate (m)
z^*	reduced axial coordinate $z^* = z/R$

Greek Letters

δ, δ'	thicknesses of liquid films (m)
$\Delta\eta_k$	radial grid spacing
Δz_i	axial grid spacing (i = 1, 2)
φ	relative humidity
ϕ	heat flux (W)
η_k	transformed radial coordinates
λ	thermal conductivity ($W.m^{-1}.K^{-1}$)
λ^*	ratio of thermal conductivities $\lambda^* = \lambda_s/\lambda_L$
μ	dynamic viscosity ($kg.m^{-1}.s^{-1}$)
ν	kinematic viscosity ($m^2.s^{-1}$)
ρ	density ($kg.m^{-3}$)

Superscripts and Subscripts

'	for quantities of external tube
0	inlet conditions
a	air
c	condensation
e	evaporation
i	liquid-mixture interface
k	phase (k = L, M, S)
L	liquid
M	vapour-gas mixture
S	solid wall
v	vapour

REFERENCES

[1] W.M. Yan, D. Lin, Int. J. Heat Mass Transfer **2001**, 44, 1143.
[2] E.H. Mezaache, M. Daguenet, Can. J. Chem. Eng. **2000**, 78, 994.
[3] M. El Armouzi,X. Chesneau, B. Zeghmati, Heat Mass Transfer **2005**, 41, 375.
[4] M. Feddaoui, E.M. Belahmidi, A. Mir, A. Bendou, Int. J. Therm. Sci. **2001**, 40, 1011.
[5] S. Ben Jabrallah, A. Belghith, J.P. Corriou, Int. J. Therm. Sci. **2006**, 45, 16.
[6] A.S. Cherif, M.A. Kassim, B. Benhamou, S. Harmand, J.P. Corriou, S. Ben Jabrallah, Int. J. Therm. Sci. **2011**, 50, 942.
[7] R. Ben Radhia, J.P. Corriou, S. Harmand, S. Ben Jabrallah, Int. J. Therm. Sci. **2011**, 50, 1996.
[8] Ch. Debbissi Hfaiedh, A. Nasr , S. Ben Nasrallah, Int. J. Therm. Sci. **2013**, 72, 34.
[9] E.C. Siow, S.J. Ormiston, H.M. Soliman, Heat Mass Transfer **2004**, 40, 365.
[10] E.C. Siow, S.J. Ormiston, H.M. Soliman, Int. J. Therm. Sci. **2007**, 46, 458.
[11] A. Belhadj Mohamed, J. Orfi, C. Debissi, S. Ben Nasrallah, Desalination **2007**, 204, 471.
[12] V. Dharma Rao, V. Murali Krishna, K.V. Sharma, P.V.J. Mohana Rao, Int. J. Heat Mass Transfer **2008**, 51, 6090.
[13] I.S. Park, M.Y. Kim, Int. J. Heat Mass Transfer **2009**, 52, 2599.
[14] C. Li, J. Li, Chinese J. Chem. Eng. **2011**, 19, 944.
[15] Y. El Hammami, M. Feddaoui, T. Mediouni, A. Mir, Heat Mass Transfer **2012**, 48, 1675.
[16] F. Hassaninejadfarahani, M.K. Guyot, S.J. Ormiston, Int. J. Heat Mass Transfer **2014**, 78, 170.
[17] S. K. Dahikar, A. A. Ganguli, M. S. Gandhi, J. B. Joshi, P. K. Vijayan, Can. J. Chem. Eng. **2013**, 91, 959.
[18] A. A. Ganguli, S. K. Dahikar, M. S. Gandhi, J. B. Joshi, P. K. Vijayan, Can. J. Chem. Eng. **2013**, 91, 974.
[19] L. Merouani, B. Zeghmati, A. Belhamri, Can. J. Chem. Eng. **2013**, 91, 1597.
[20] A. Dehbi, F. Janasz, B. Bell, Nucl. Eng. Des. **2013**, 258, 199.
[21] Z. Zhao, Y. Li, K. Zhu, Y. Ma, Can. J. Chem. Eng. **2015**, 93, 2253.
[22] A. Dehbi, Int. J. Heat Mass Transfer **2015**, 86, 1.
[23] B.E. Poling, J.M. Prausnitz, J.P. O'Connell, The Properties of Gases and Liquids, Fifth Edition, McGraw– Hill, New-York **2004**.

List of figures

Figure 1. Physical model
Figure 2. Numerical domain and discretization grid
Figure 3. Comparison of present model with results of Feddaoui et al.[4]
Figure 4. Comparison of present model with results of Dharma Rao et al.[12]
Figure 5. Velocity profiles at various sections for the inner mixture and the evaporating liquid film
Figure 6. Velocity profiles at various sections for the outer mixture and the condensing liquid film
Figure 7. Temperature profiles at various sections
Figure 8. Vapour concentration profiles at various sections
Figure 9. Effect of Re_0 on the evaporation rate
Figure 10. Effect of Re_0 on the condensation rate
Figure 11. Effect of Re_0 on the heat flux
Figure 12. Effect of φ_0 on the evaporation rate
Figure 13. Effect of φ_0 on the condensation rate
Figure 14. Effect of φ_0 on the heat flux
Figure 15. Effect of P_0 on the evaporation rate
Figure 16. Effect of P_0 on the condensation rate
Figure 17. Effect of P_0 on the heat flux
Figure 18. Effect of q_{L0} on the evaporation rate
Figure 19. Effect of q_{L0} on the condensation rate
Figure 20. Effect of q_{L0} on the heat flux

List of tables

Table 1. Diffusion coefficients $\Gamma_{\psi k}$ and source terms $S_{\psi k}$ in the conservation equations

Table 1. Diffusion coefficients $\Gamma_{\psi k}$ and source terms $S_{\psi k}$ in the conservation equations

Fluid	Equation	ψ_k	$\Gamma_{\psi k}$	$S_{\psi k}$
Liquid films (k = L)	Momentum	U_L	μ_L	$\rho_L g - \frac{dP}{dz}$
	Energy	T_L	λ_L/c_{pL}	0
Vapour-gas mixtures (k = M)	Momentum	U_M	μ_M	$\rho_M g - \frac{dP}{dz}$
	Energy	T_M	λ_M/c_{pM}	ϕ_{ed}
	Diffusion	C	$\rho_M D_v$	0

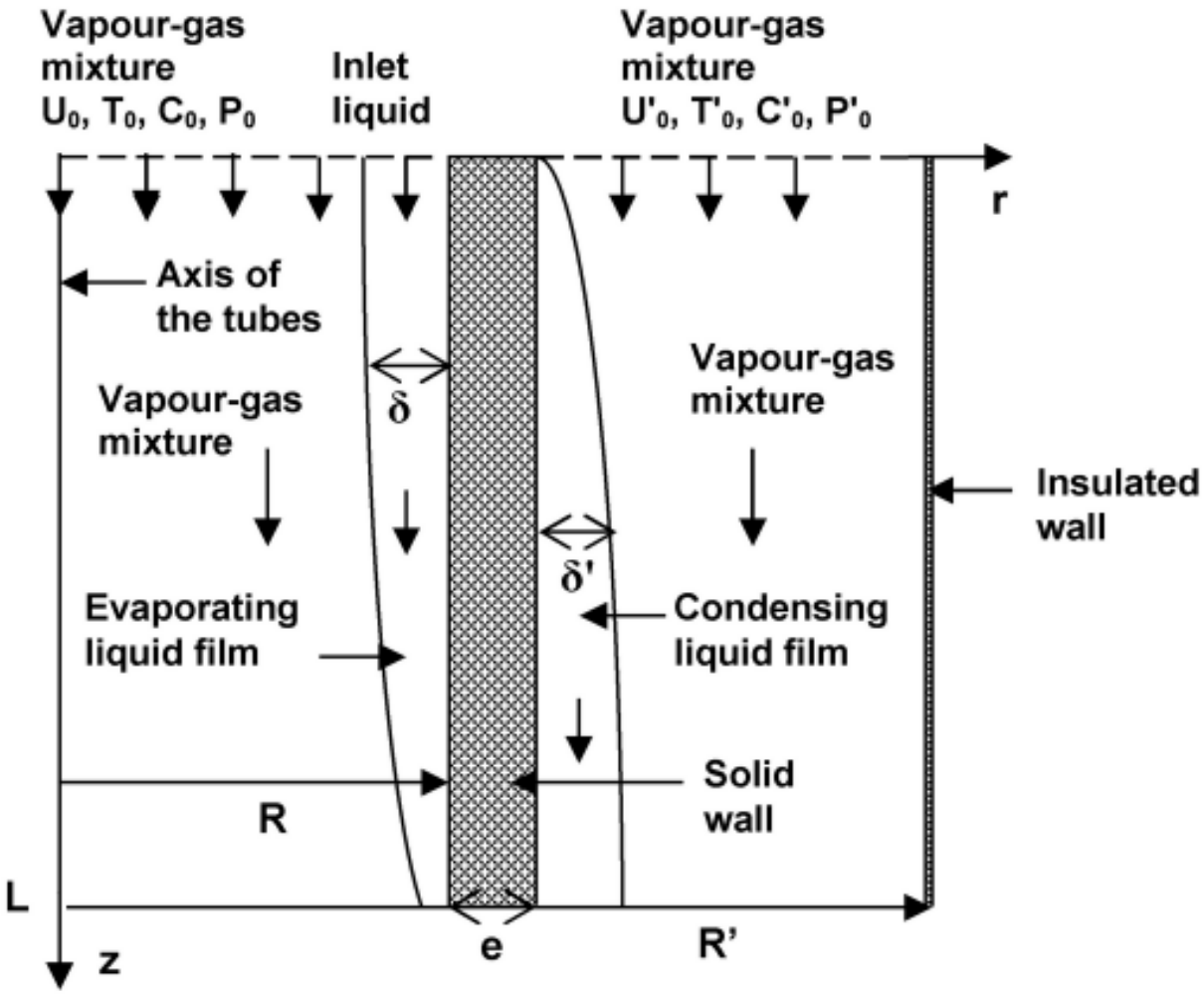

Figure 1

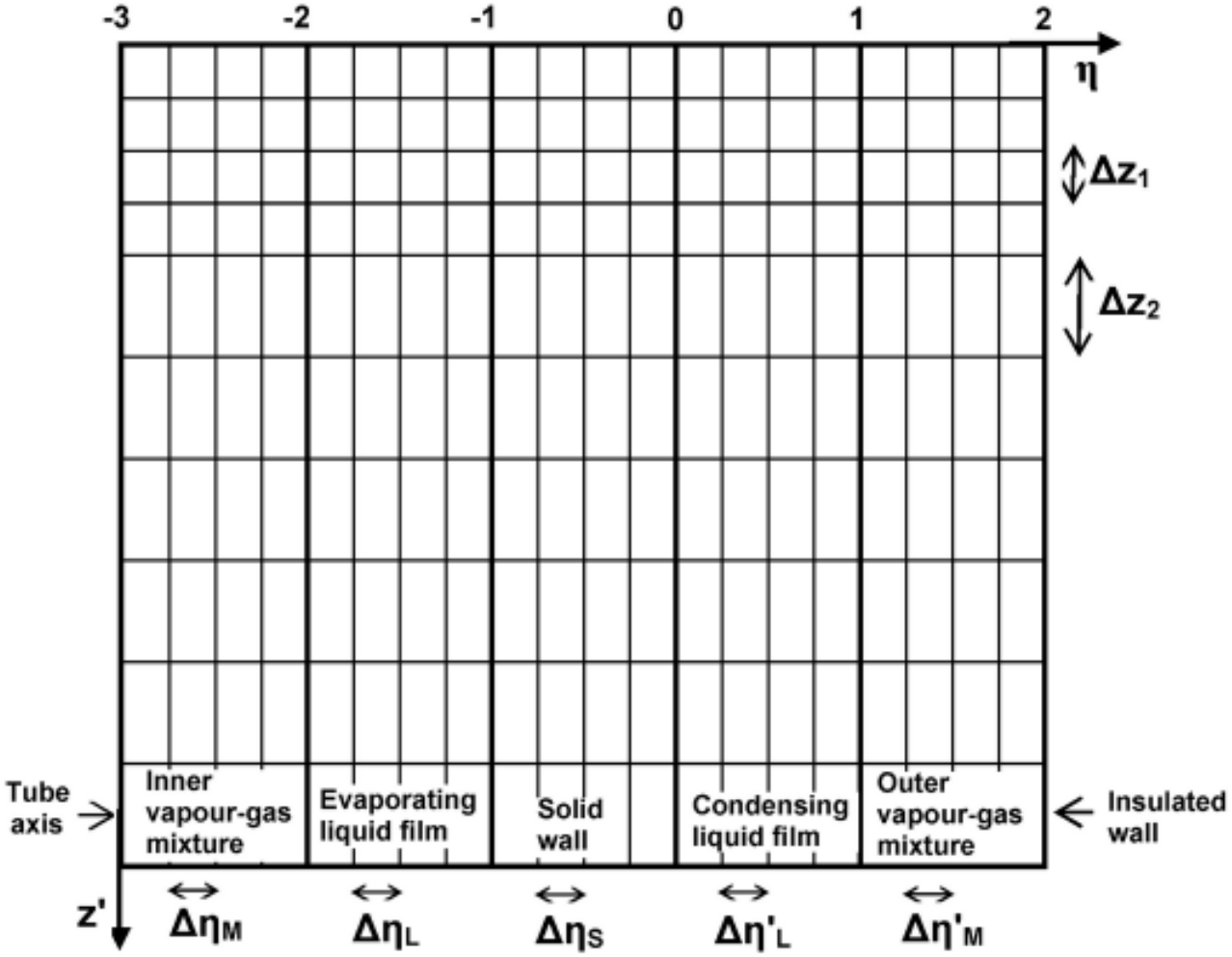

Figure 2

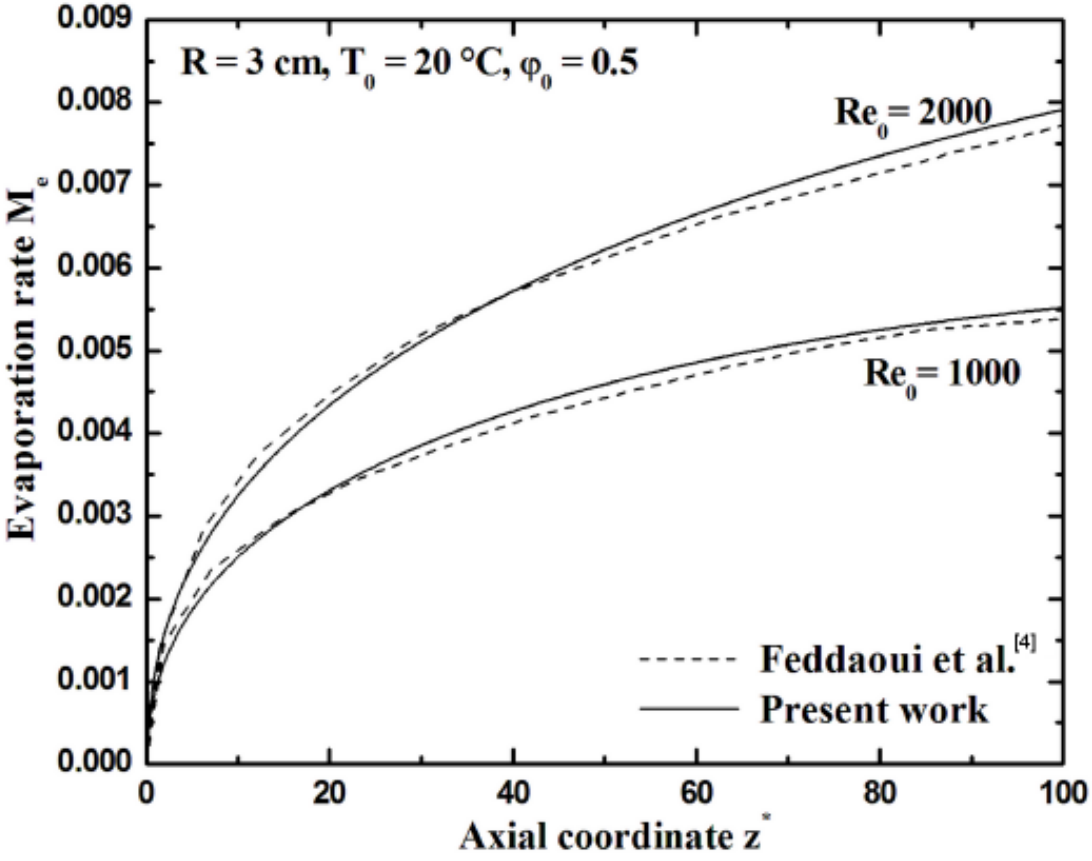

Figure 3

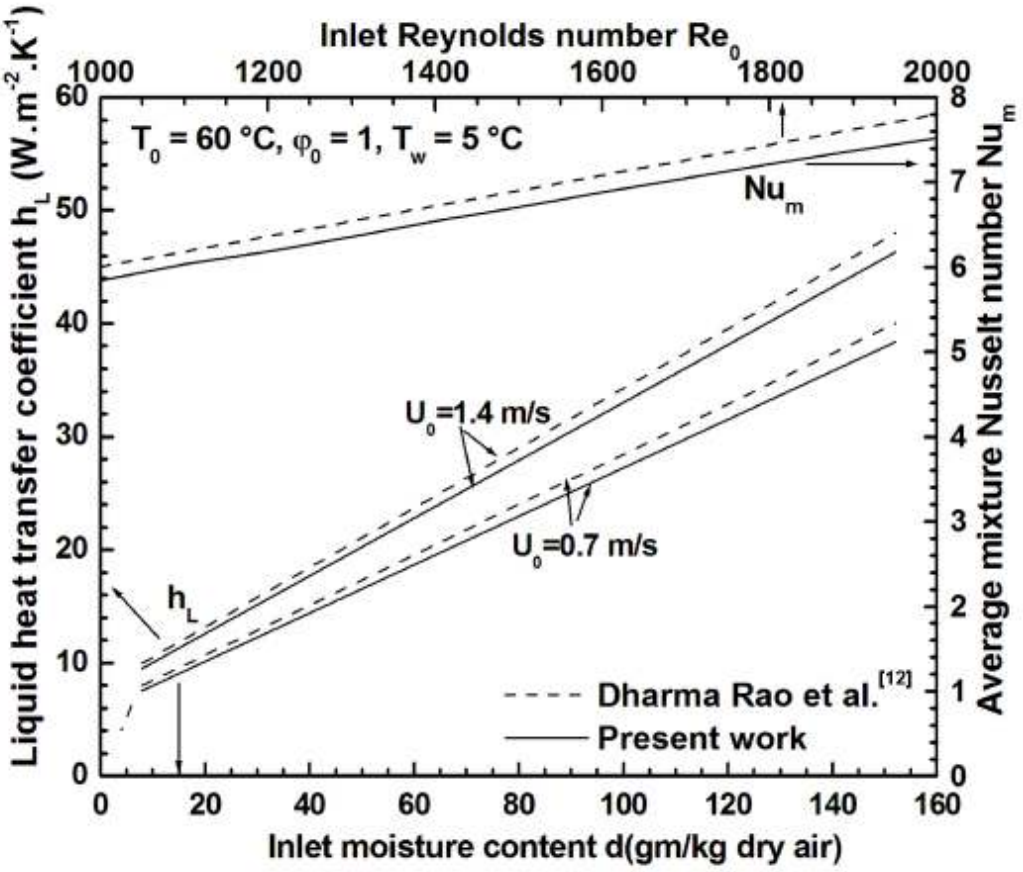

Figure 4

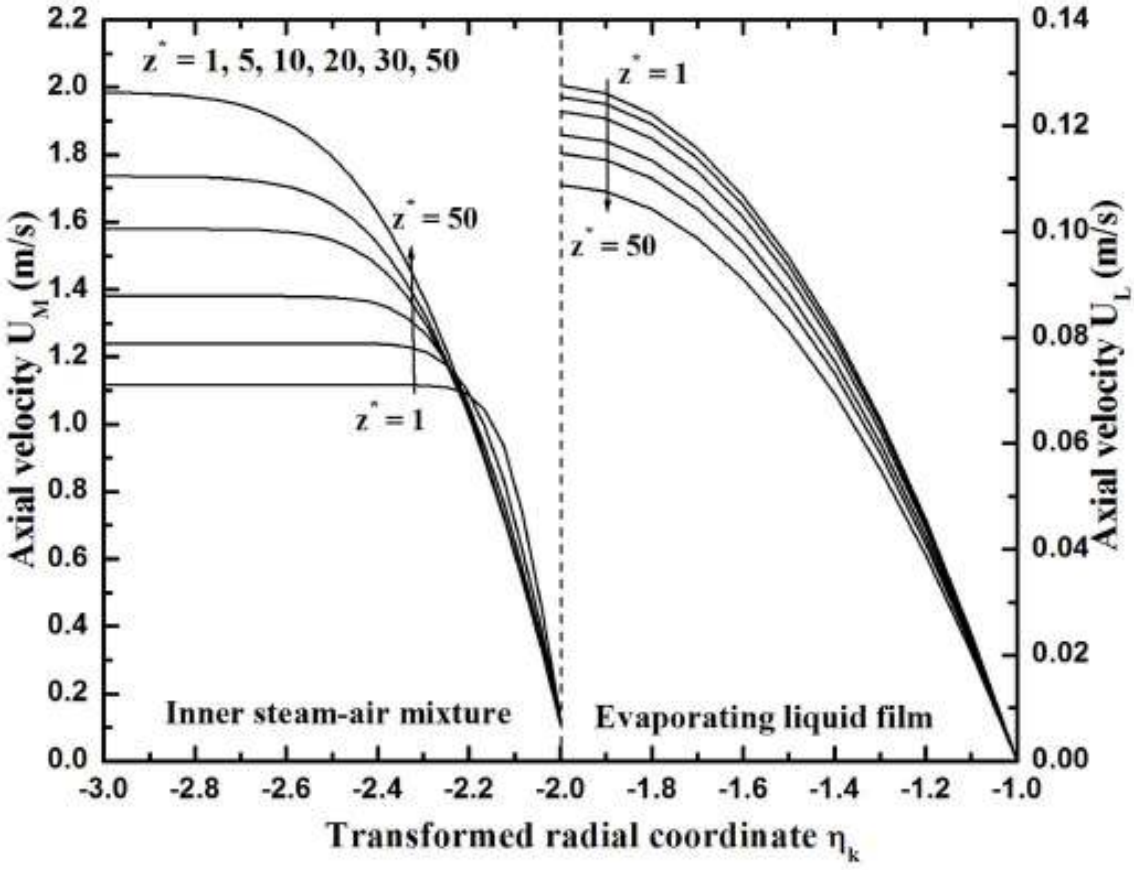

Figure 5

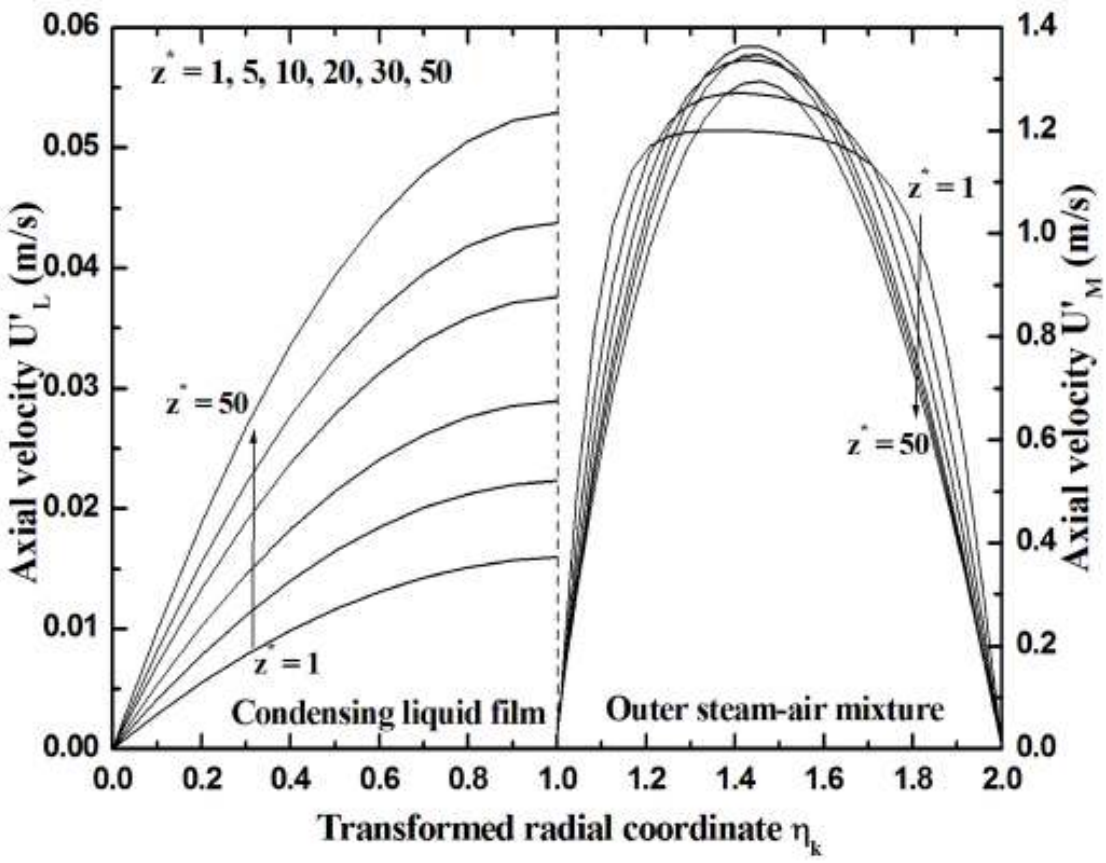

Figure 6

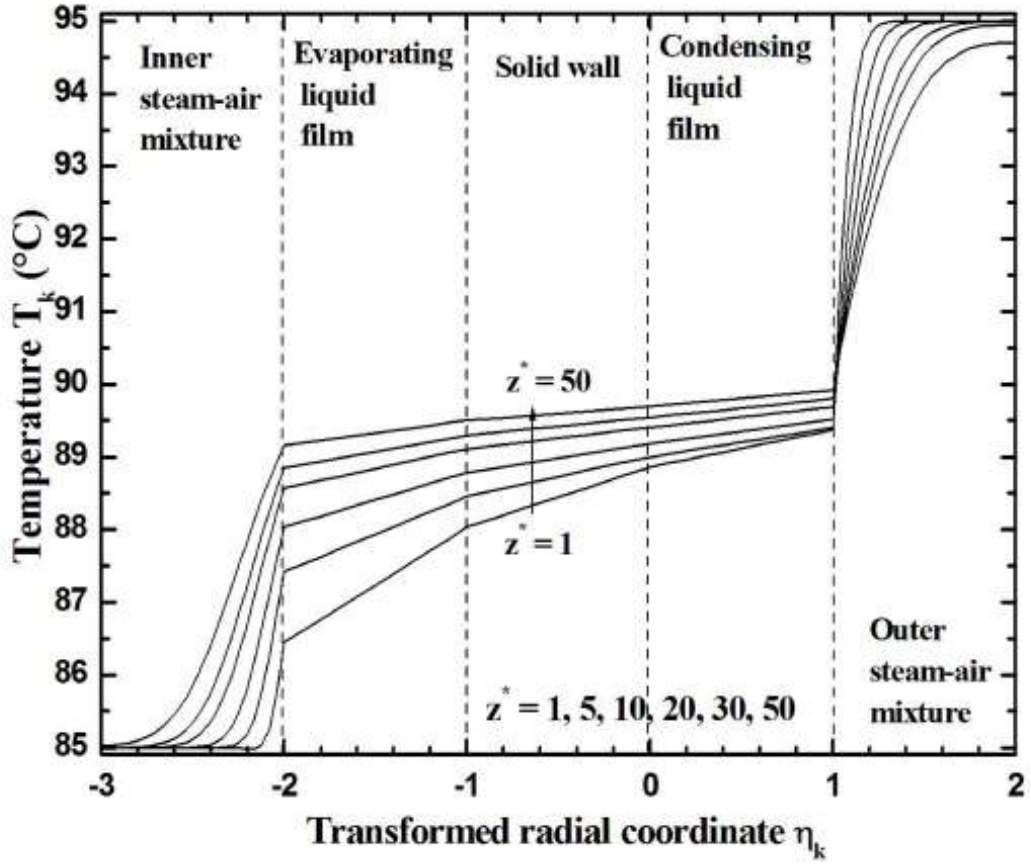

Figure 7

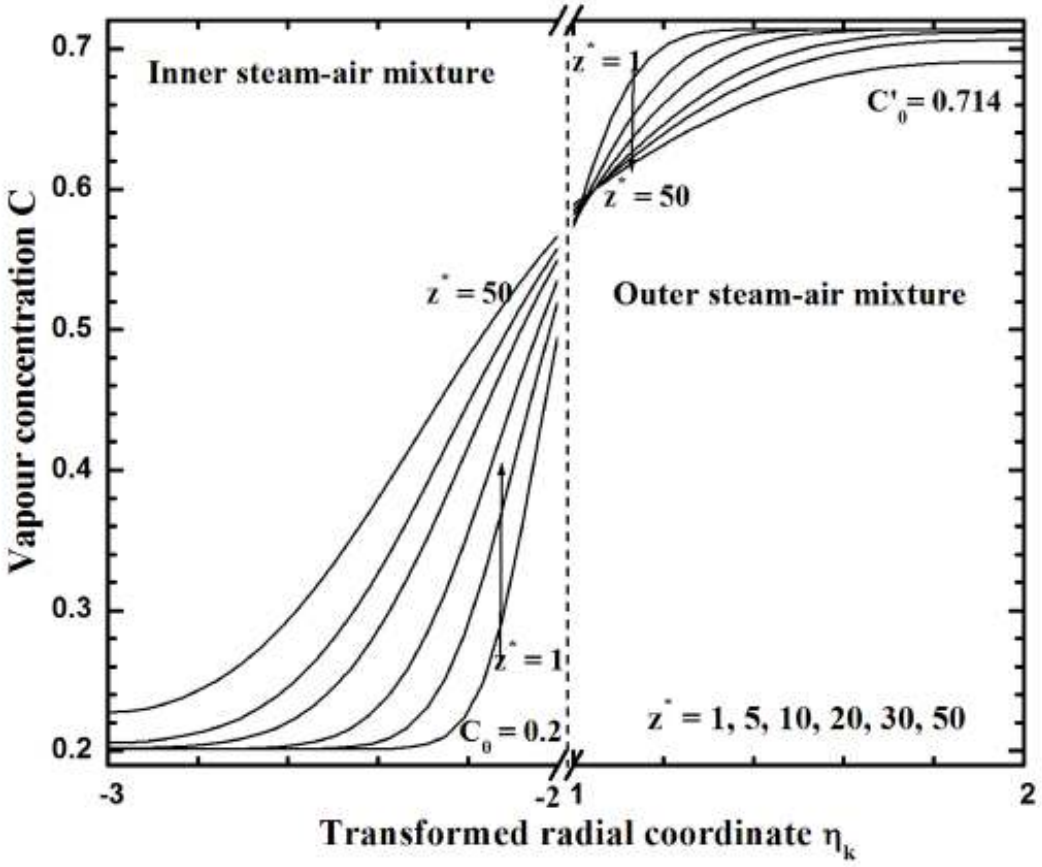

Figure 8

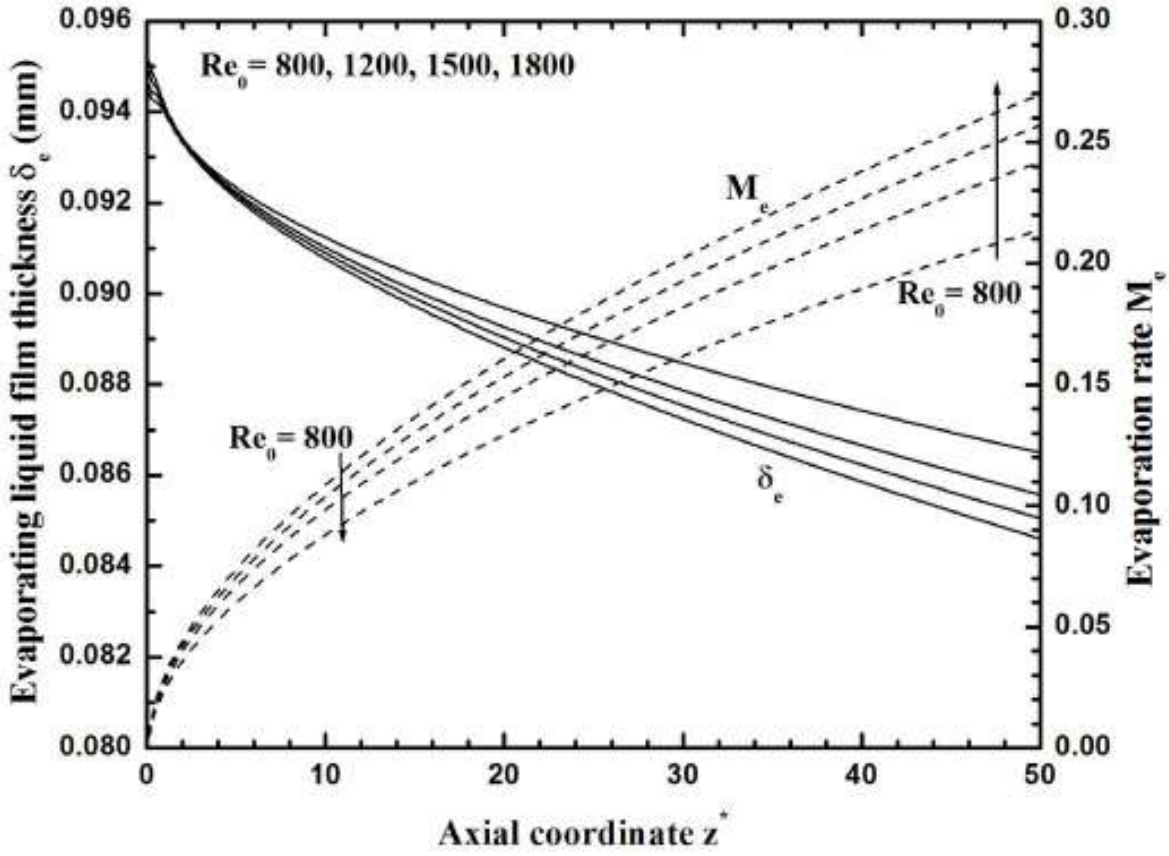

Figure 9

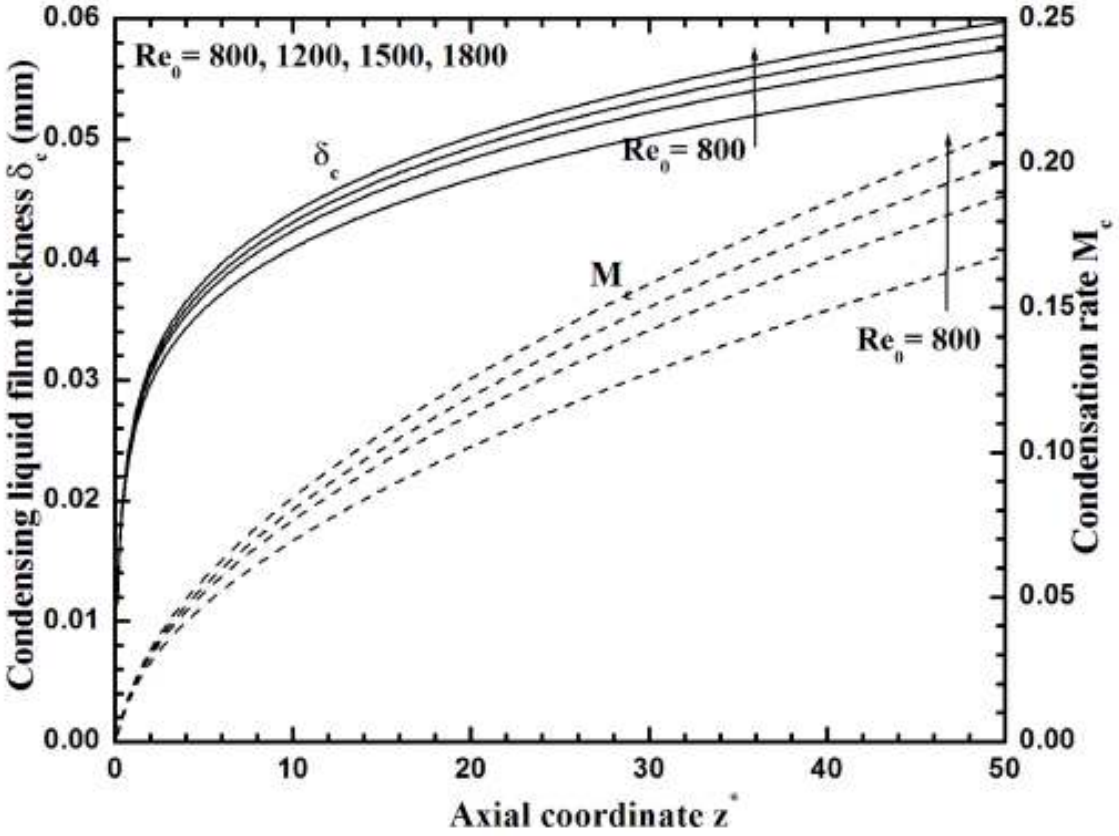

Figure 10

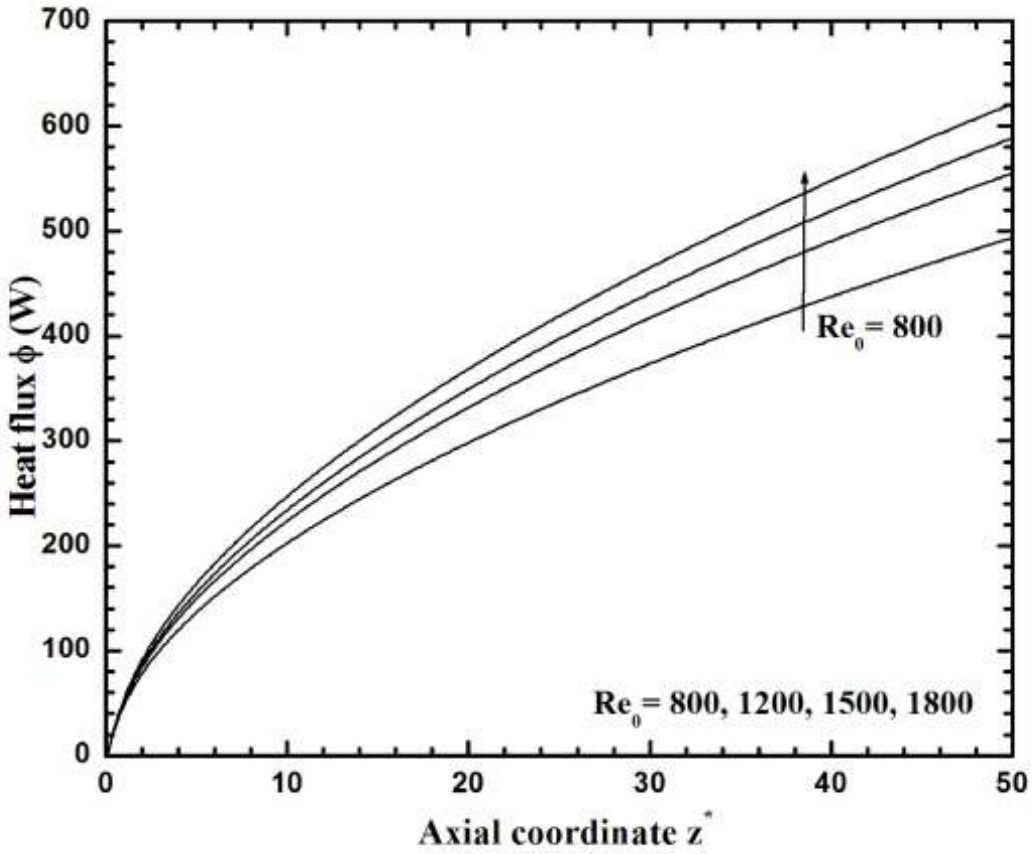

Figure 11

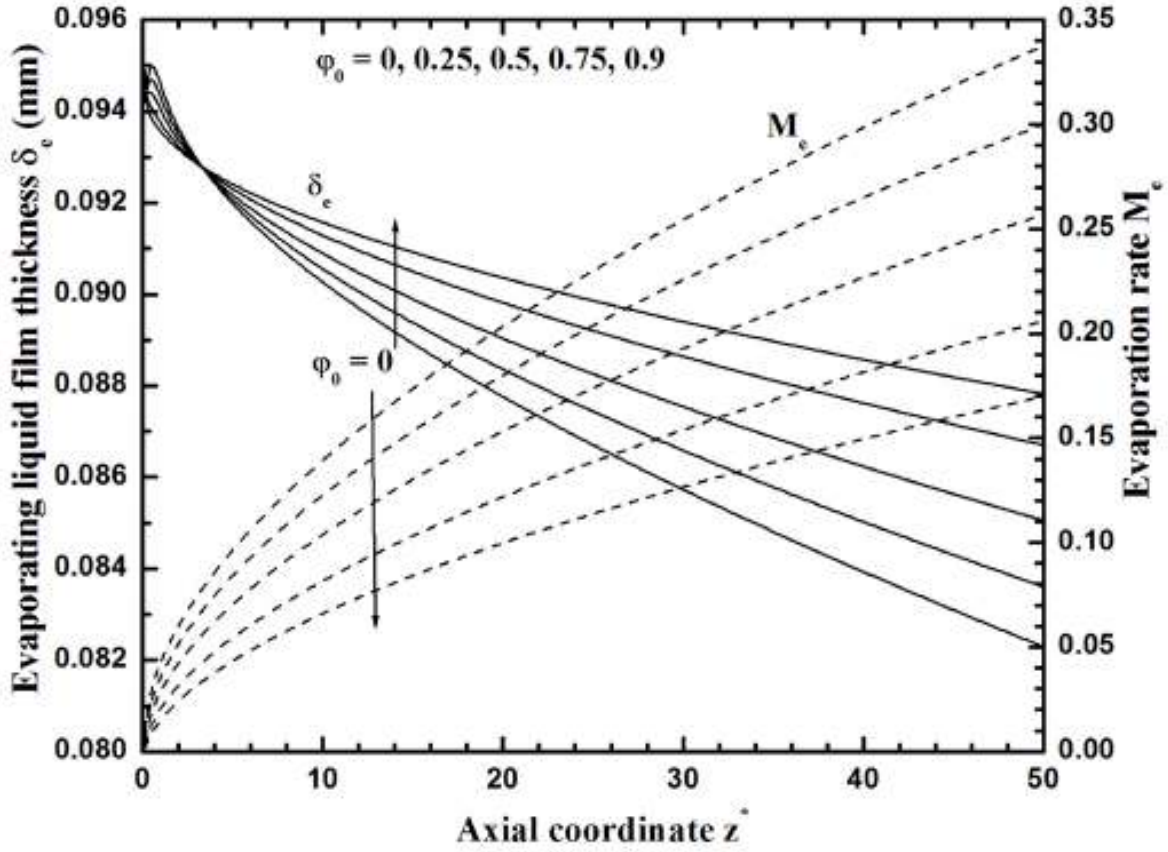

Figure 12

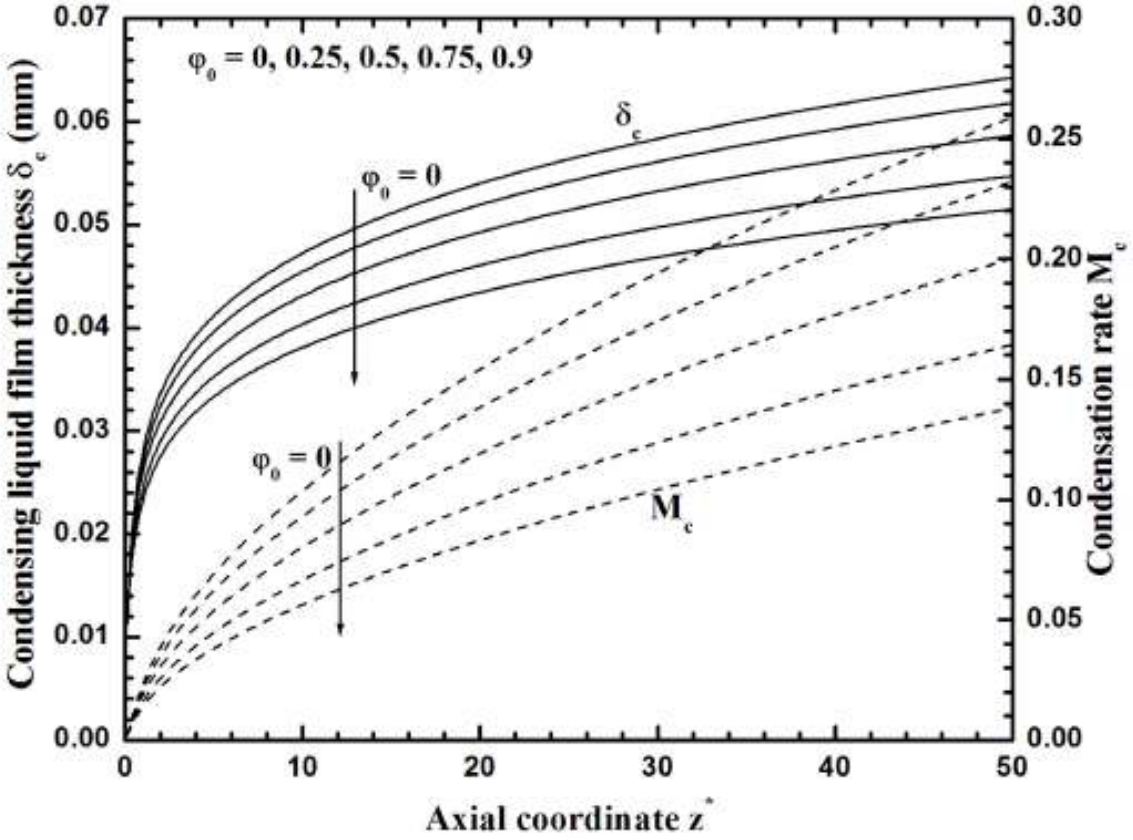

Figure 13

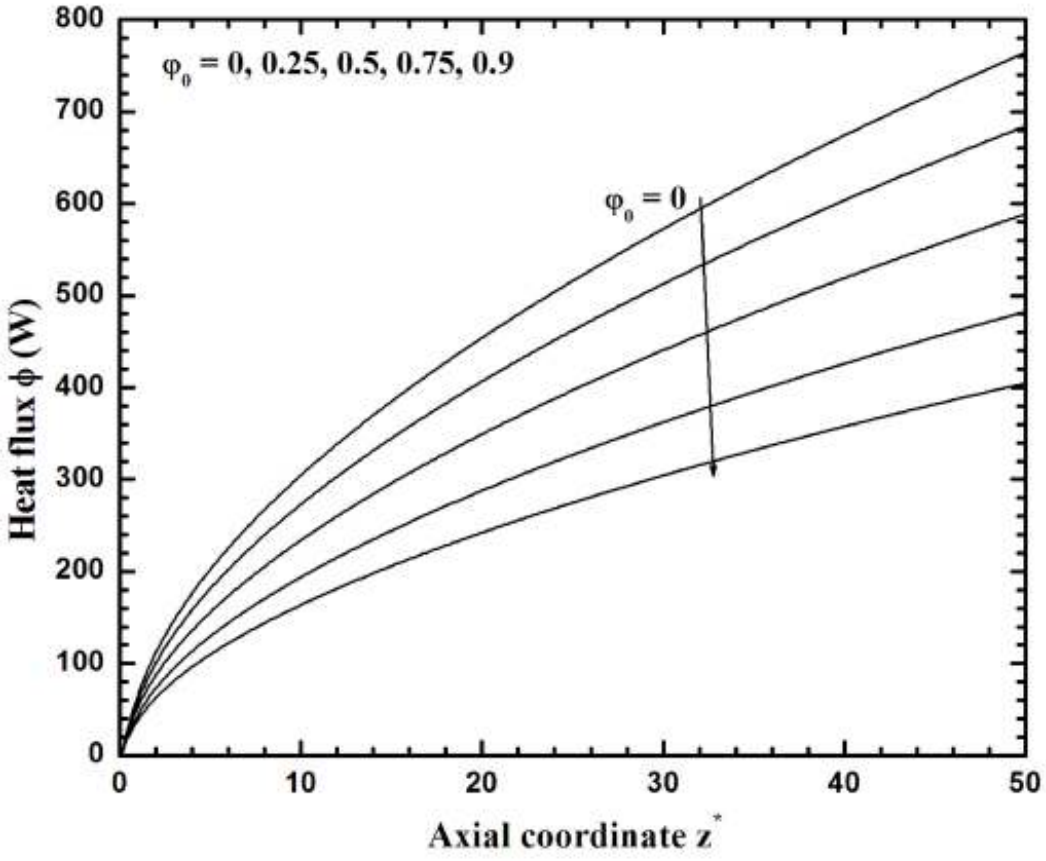

Figure 14

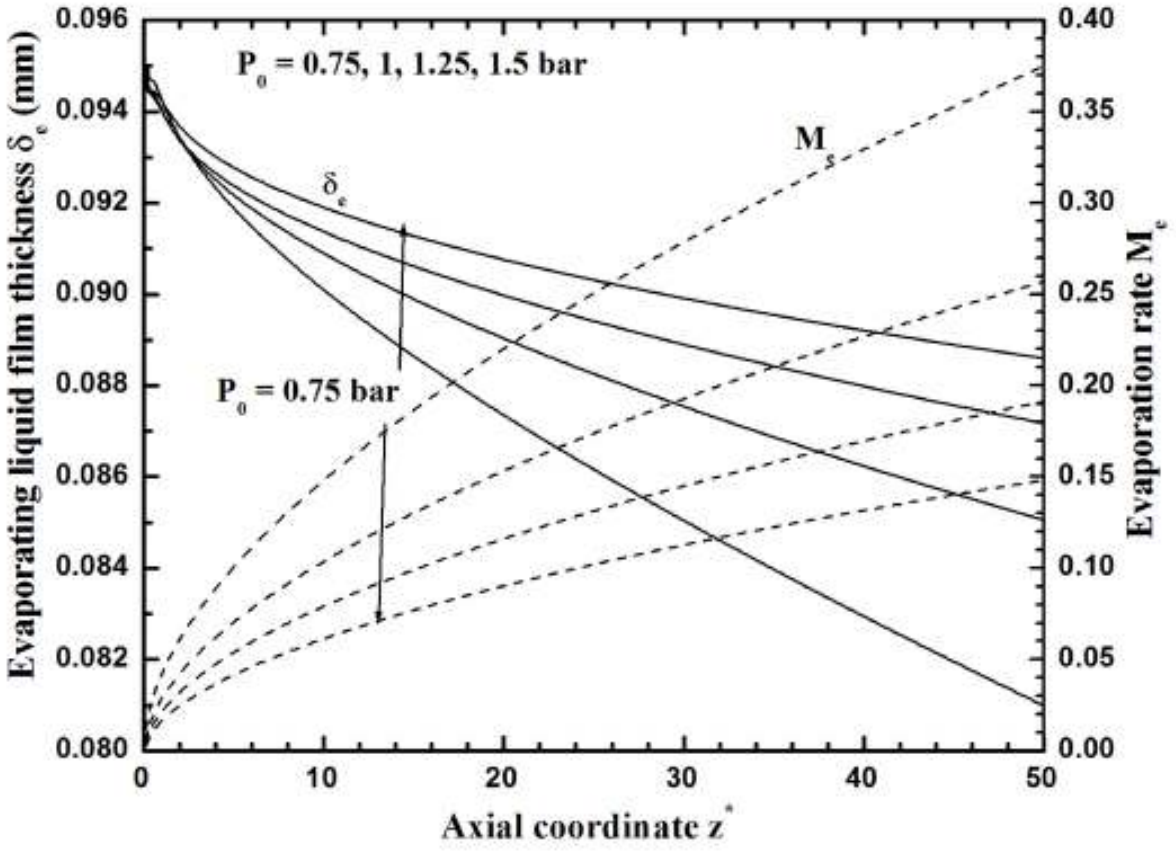

Figure 15

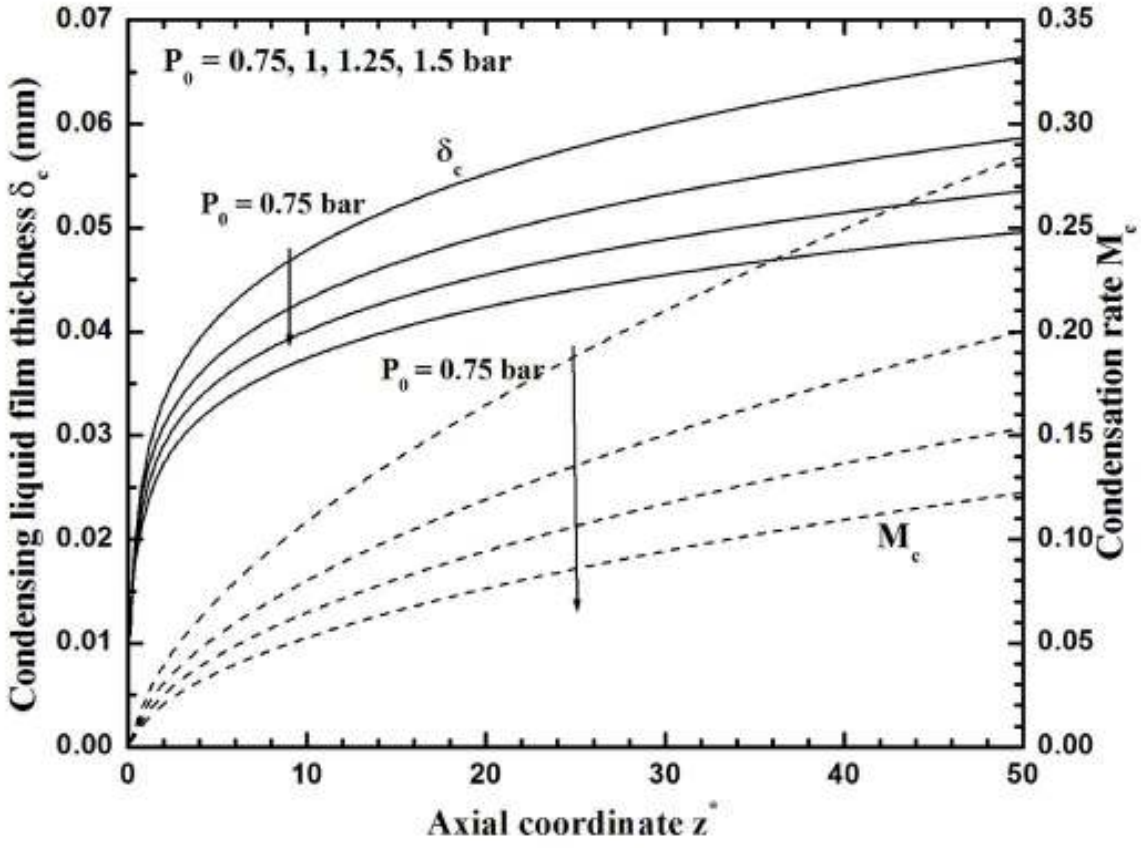

Figure 16

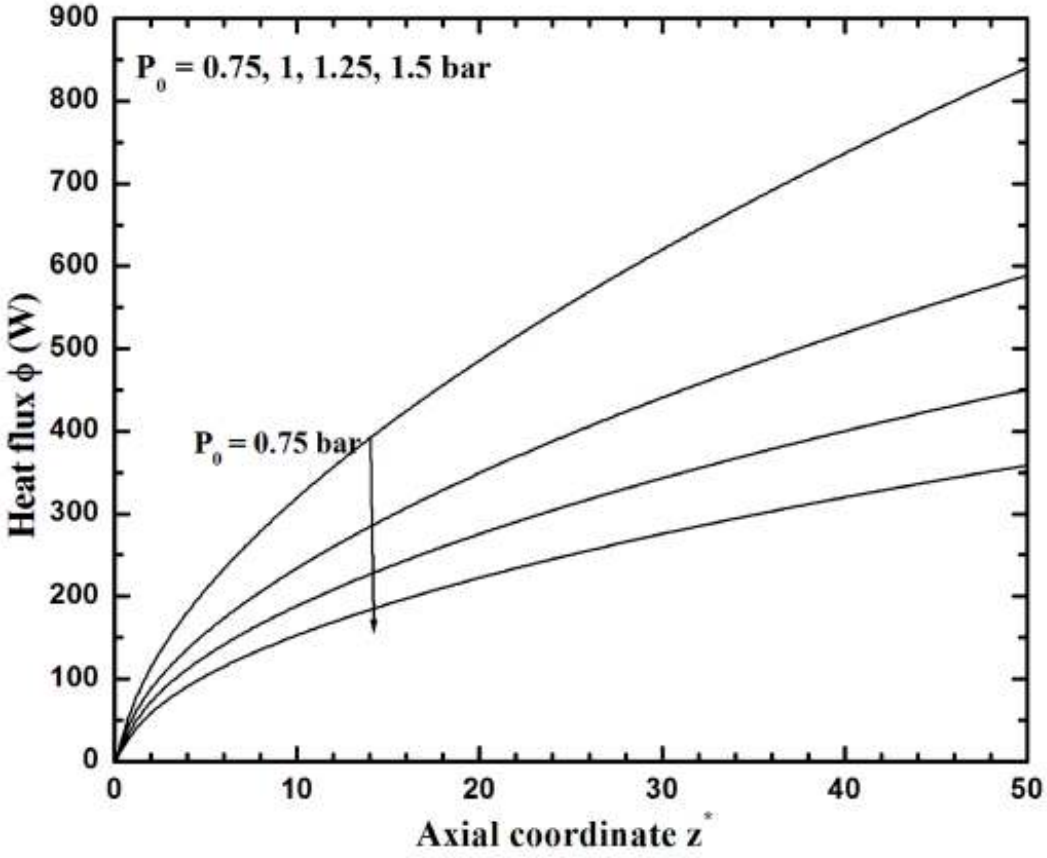

Figure 17

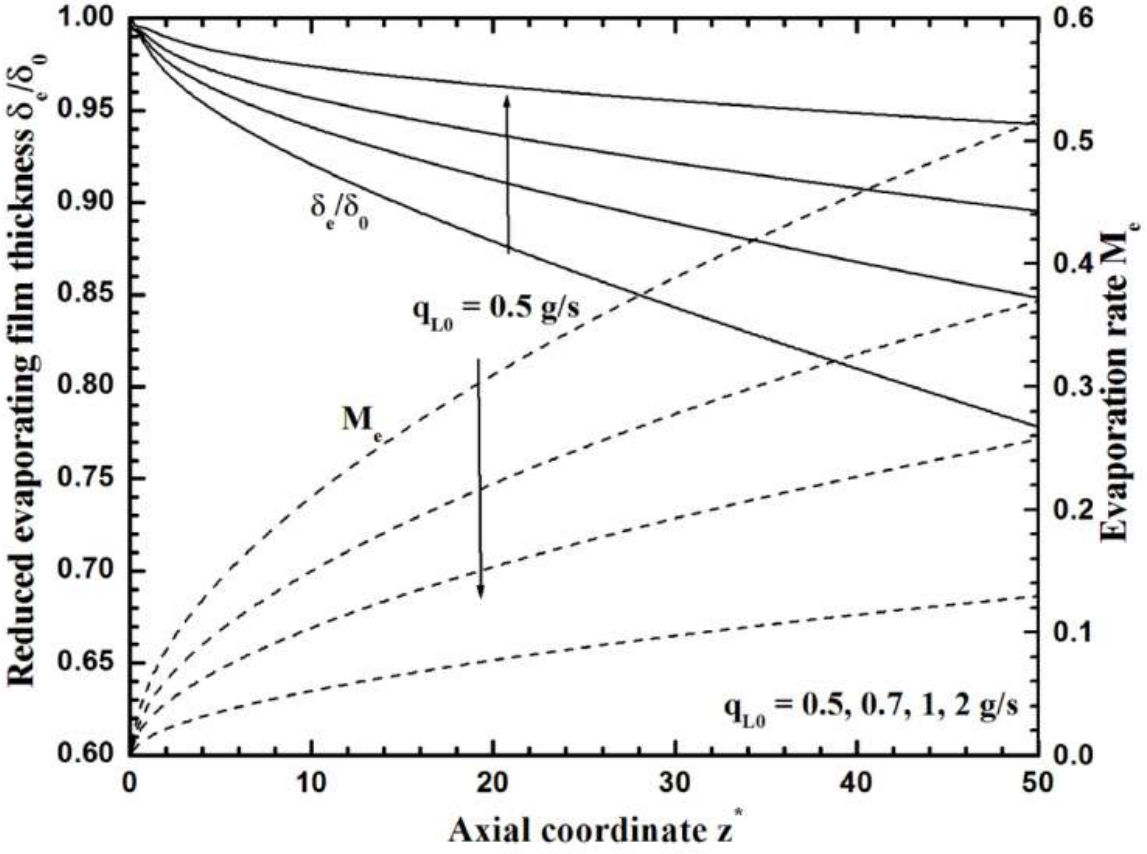

Figure 18

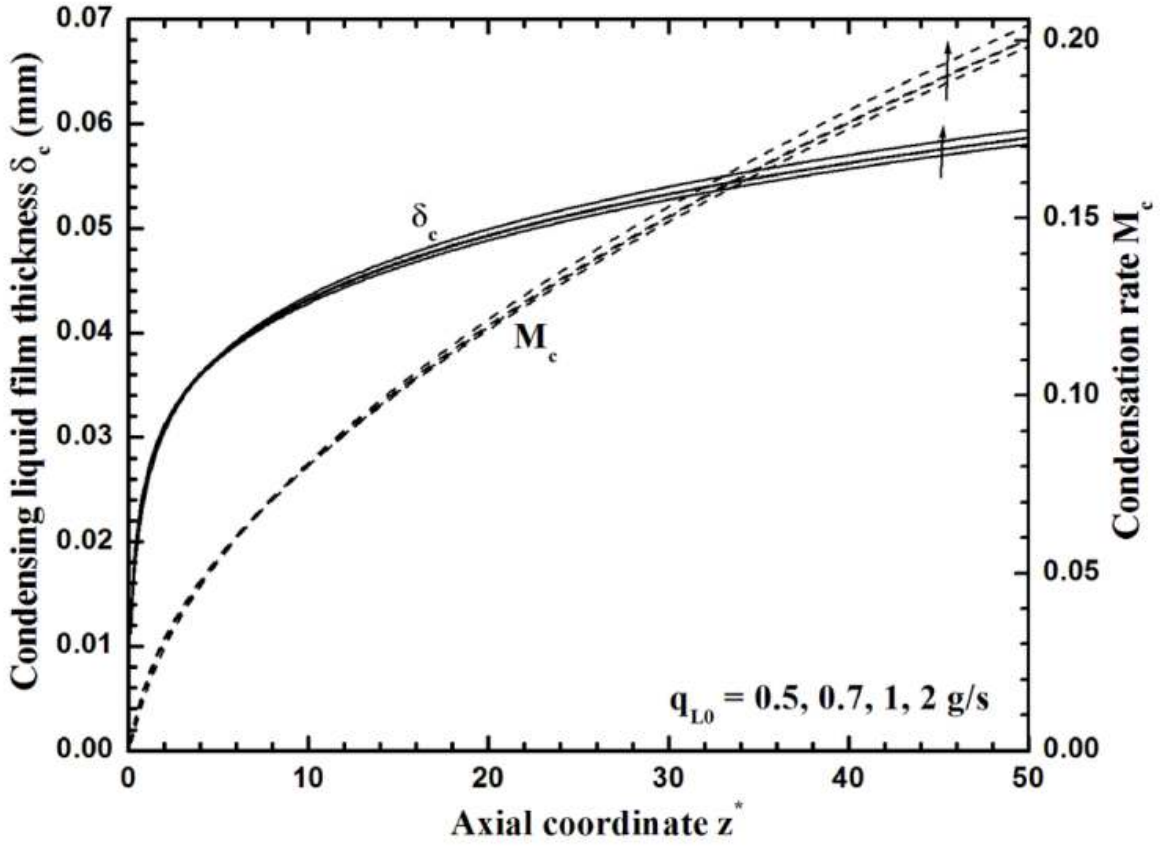

Figure 19

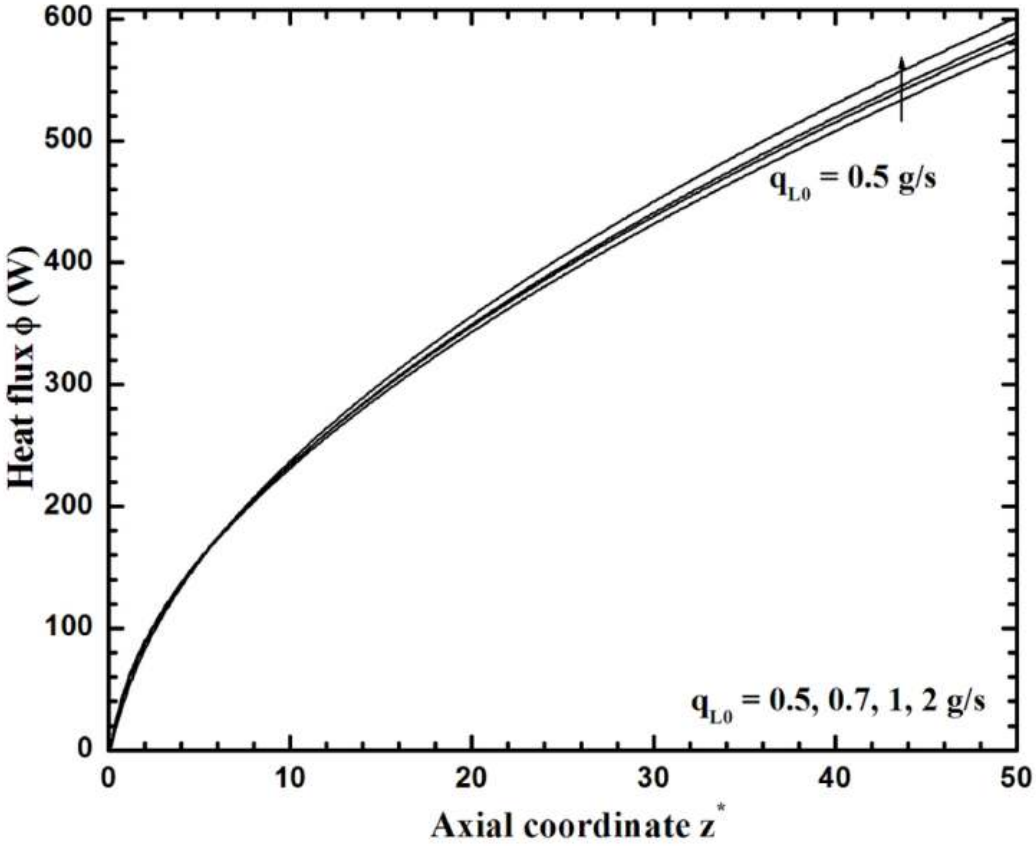

Figure 20